Supporting Information

Banci et al. 10.1073/pnas.1010095107

SI Text

yTim10 Protein Production. Wild-type yeast Tim10 gene is inserted into pGEX plasmid to generate the N-terminal GST-fused protein. A thrombin recognition site was present between the GST tag and the Tim10 gene for cleavage of the GST tag. Wild-type yTim10 protein was expressed in *Escherichia coli* BL21(DE3) gold cells (Stratagene) grown in Luria–Bertani or in minimal medium in the presence of $[(^{15}NH_4)_2SO_4]$ for the production of ^{15}N-labeled samples. Protein expression was induced with 0.4 mM IPTG for 4 h at 303 K. Purification was performed by using a GSTrap™ column (GE Healthcare Life Sciences). The GST tag was cleaved with thrombin protease and separated from yTim10 with a size exclusion chromatography using a HiLoad 16/60 Superdex 75 pg (Amersham Pharmacia Biosciences) gel filtration column. The protein concentration was measured using the Bradford protein assay. Unlabeled and ^{13}C,^{15}N-labeled samples of yTim10 mutant were produced and purified similarly to the wild-type protein.

The synthetic peptide RLYSNLVERC representing the internal targeting signal (ITS) sequence of yTim9 protein was purchased (Ansynth Service), HPLC-purified, and N-terminally acetylated.

CD. Far-UV CD spectra (190–260 nm) on wild-type yTim10, C44/61/65S yTim10, and yTim9 peptide were recorded on a JASCO J-810 spectropolarimeter. Each spectrum was obtained as the average of four scans and corrected by subtracting the contributions from the buffer. Each sample was in 50 mM phosphate buffer, EDTA 0.5 mM, pH 7.0. All of the steps were performed under nitrogen atmosphere using a degassed buffer. Quantitative estimate of the secondary structure contents was made by using the DICROPROT software package.

In-Cell NMR. *E. coli* cells harboring the plasmid encoding the yCox17 gene were first grown in unlabeled LB medium. Protein expression was then induced after resuspending the bacterial cells into stable ^{15}N isotope-labeled medium (100 mL). The collected cells were placed as 60% slurry into NMR tubes. Sample stability was monitored repeatedly by recording 2D ^{1}H-^{15}N HSQC spectra at various times, followed by plating colony tests. It is crucial for in-cell NMR to ensure that the proteins providing the signals in the NMR spectra are inside the living cells and that the contribution from extracellular proteins is negligible. To check this aspect, ^{1}H-^{15}N HSQC spectra were performed on the growth medium after removal of the bacterial cells by gentle centrifugation. Cross-peaks were absent, at variance with the ^{1}H-^{15}N HSQC spectra of bacterial cells, indicating that the presence of extracellular proteins is negligible. This result was confirmed by SDS-PAGE of the extracellular and cellular fractions. On the contrary, the spectrum of lysed cells shows cross-peaks sharper than those in the cell and with backbone chemical shifts typical of the oxidized state of yeast Cox17 ($Cox17_{2S–S}$).

NMR Spectroscopy. NMR experiments were acquired using Bruker Avance spectrometers operating at proton frequencies of 500, 700, 800, and 900 MHz, all equipped with cryoprobes. All NMR samples were in 50 mM phosphate buffer, EDTA 0.5 mM, pH 7.0. ^{1}H, ^{13}C, ^{15}N backbone resonances of C53S hMia40 in both free and substrate bound states, as well as of C26/36/55S hCox17 and C44/61/65S yTim10 mutants in both free and hMia40-bound states, were assigned, performing all the typical triple resonance experiments for backbone assignment. ^{13}C-edited and ^{15}N-edited HSQC-NOESY experiments were then acquired for side-chain and NOE assignments on the C26/36/55S hCox17-C53S hMia40 complex, where ^{13}C and ^{15}N labeling is present, respectively, on C26/36/55S hCox17 or on C53S hMia40. Two-dimensional total correlation spectroscopy (TOCSY) maps with ^{1}H-^{13}C filtering in the two dimensions and 2D NOESY maps with ^{1}H-^{15}N filtering in the two dimensions were also acquired to identify intramolecular bond correlations and NOEs within the unlabeled partner (1). The ^{1}H, ^{15}N, ^{13}C resonances of the unlabeled yTim9 peptide (RLYSNLVERC) in the free state were assigned through rotating-frame Overhauser effect spectroscopy, TOCSY, and ^{1}H-^{13}C HSQC, ^{1}H-^{15}N HSQC spectra. ^{1}H resonances of the unlabeled yTim9 peptide covalently bound to ^{13}C, ^{15}N C53S Mia40 were assigned through 2D TOCSY maps with ^{1}H-^{13}C filtering in the two dimensions and a 2D NOESY map with ^{1}H-^{15}N filtering in the two dimensions (1).

To identify intermolecular NOEs in the C26/36/55S hCox17-C53S hMia40 complex, a $\omega 1$-^{13}C-edited, $\omega 2$-^{13}C-filtered NOESY experiment (1) was recorded in a 2D plane (^{1}H-^{1}H plane) (Fig. S7) on two samples—i.e., ^{13}C, ^{15}N C26/36/55S hCox17/unlabeled C53S hMia40 and ^{13}C, ^{15}N C53S hMia40/unlabeled C26/36/55S hCox17.

^{1}H, ^{13}C, ^{15}N backbone resonances of C26/55S hCox17 were assigned, performing all the typical experiments for backbone assignment. C26/55S hCox17 forms a disulfide bond between Cys40 and Cys 45 ($C26/55S\ hCox17_{1S–S}$), as monitored from their ^{13}C chemical shift values (2). Secondary structure elements of C26/55S hCox17 were determined through chemical shift index and PECAN programs (3, 4).

1. Zwahlen C, et al. (1997) Methods for measurement of intermolecular NOEs by multinuclear NMR spectroscopy: Application to a bacteriophage N-peptide/*boxB* RNA complex. *J Am Chem Soc* 119:6711–6721.
2. Sharma D, Rajarathnam K (2000) ^{13}C NMR chemical shifts can predict disulfide bond formation. *J Biomol NMR* 18:165–171.
3. Wishart DS, Sykes BD, Richards FM (1992) The chemical shift index: A fast and simple method for the assignment of protein secondary structure through NMR spectroscopy. *Biochemistry* 31:1647–1651.
4. Eghbalnia HR, et al. (2005) Protein energetic conformational analysis from NMR chemical shifts (PECAN) and its use in determining secondary structural elements. *J Biomol NMR* 32:71–81.

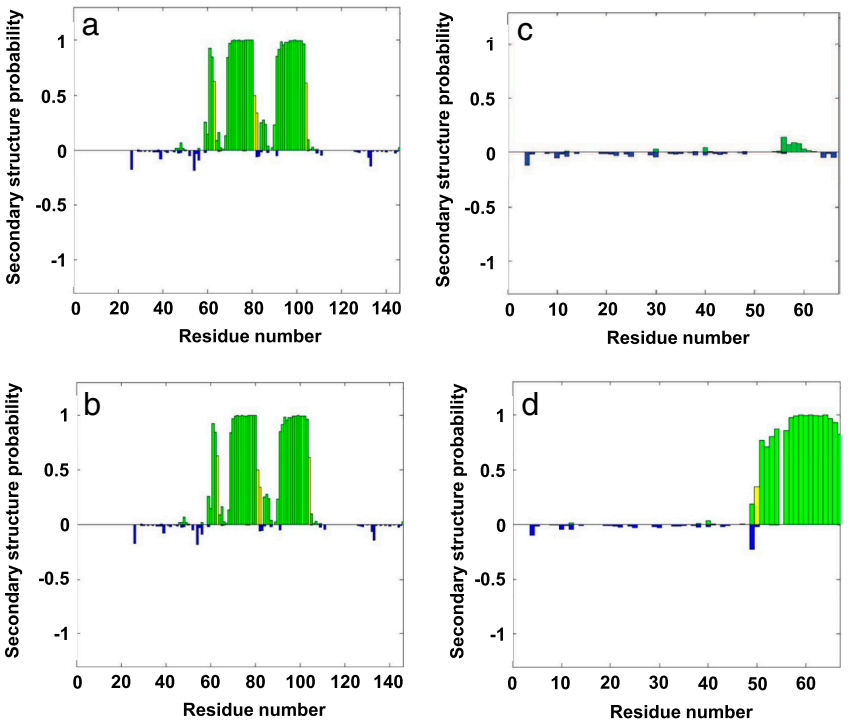

Fig. S1. Secondary structure probability of C53S hMia40 and C26/36/55S hCox17 in their free and complexed states derived from chemical shifts using the PECAN program. (*A*) Free C53S hMia40, (*B*) C53S hMia40 complexed with C26/36/55S hCox17, (*C*) free C26/36/55S hCox17, and (*D*) C26/36/55S hCox17 complexed with C53S hMia40. The vertical axis represents the probability of helix (positive, green) and of extended structure (negative, blue). Values near zero represent random coil residues. The yellow bars indicate identification of a region without a distinct structural designation. The residue numbering comprises four additional residues at the N terminus as a consequence of the cloning procedure.

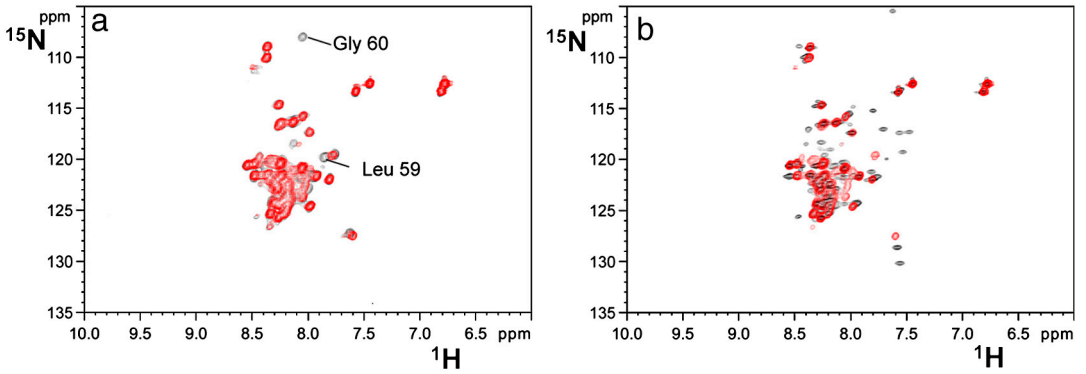

Fig. S2. Monitoring the noncovalent Cox17–Mia40 interaction. (*A*) ^{1}H-^{15}N HSQC spectrum, acquired at 500 MHz, of a 1:1 mixture of unlabeled C53S hMia40 and ^{15}N-labeled C26/36/55S hCox17 in the presence of 10 mM DTT (red) is overlaid with a ^{1}H-^{15}N HSQC spectrum, acquired at 500 MHz, of fully reduced hCox17 ($hCox17_{65H}$) (black). Residues showing broadening beyond detection are indicated. (*B*) ^{1}H-^{15}N HSQC spectrum, acquired at 500 MHz, of a 1:1 mixture of unlabeled C53S hMia40 and ^{15}N-labeled C26/36/55S hCox17 in the presence of 10 mM DTT (red) is overlaid with a ^{1}H-^{15}N HSQC spectrum, acquired at 800 MHz, of the C53S hMia40-^{15}N-labeled C26/36/55S hCox17 covalent complex (black).

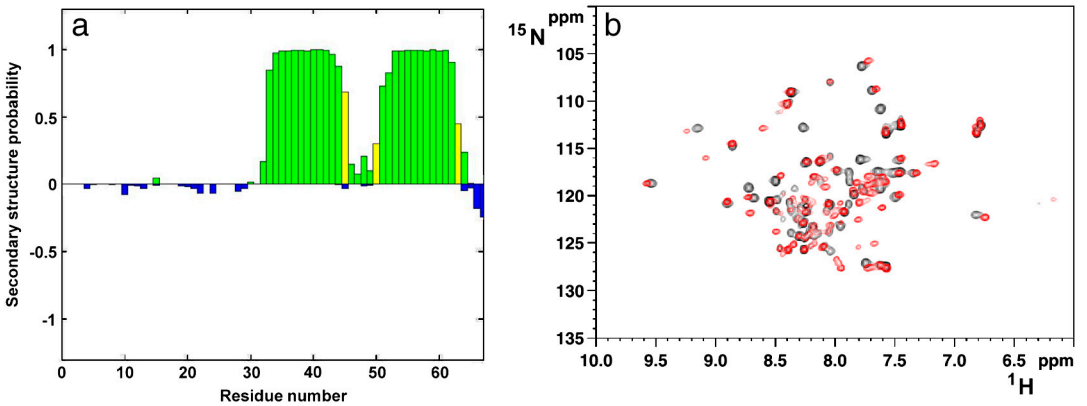

Fig. S3. Structural analysis of C26/55S hCox17$_{1S-S}$. Secondary structure elements in C26/55S hCox17$_{1S-S}$ (*A*) as obtained from chemical shifts using the PECAN program. The vertical axis represents the probability of helix (positive, green) and of extended structure (negative, blue). Values near zero represent random coil residues. The yellow bars indicate identification of a region without a distinct structural designation. The residue numbering comprises four additional residues at the N terminus as a consequence of the cloning procedure. (*B*) Overlay of ^{1}H-^{15}N HSQC spectra of C26/55S hCox17 (black) and wild-type hCox17$_{2S-S}$ (red).

a

	AA	δ HN (ppm)	δ N (ppm)	δ HA (ppm)	δ CA (ppm)	δ CB (ppm)	*Secondary structure from CSI*
1	R	8.15	126.6	4.09	56.0	30.5	*Coil*
2	L	8.17	123.3	4.20	54.8	42.2	*Coil*
3	Y	8.10	120.7	4.48	54.9	38.3	*Coil*
4	S	8.09	116.6	4.28	58.0	63.6	*Coil*
5	N	8.33	120.6	4.58	57.4	38.5	*Coil*
6	L	8.03	121.9	4.21	55.2	42.0	*Coil*
7	V	7.90	120.7	3.97	62.1	32.5	*Coil*
8	E	8.30	124.5	4.17	56.2	30.2	*Coil*
9	R	8.26	122.7	4.24	55.8	30.4	*Coil*
10	*C*	*7.94*	*124.9*	*4.26*	*59.1*	*28.8*	*Coil*

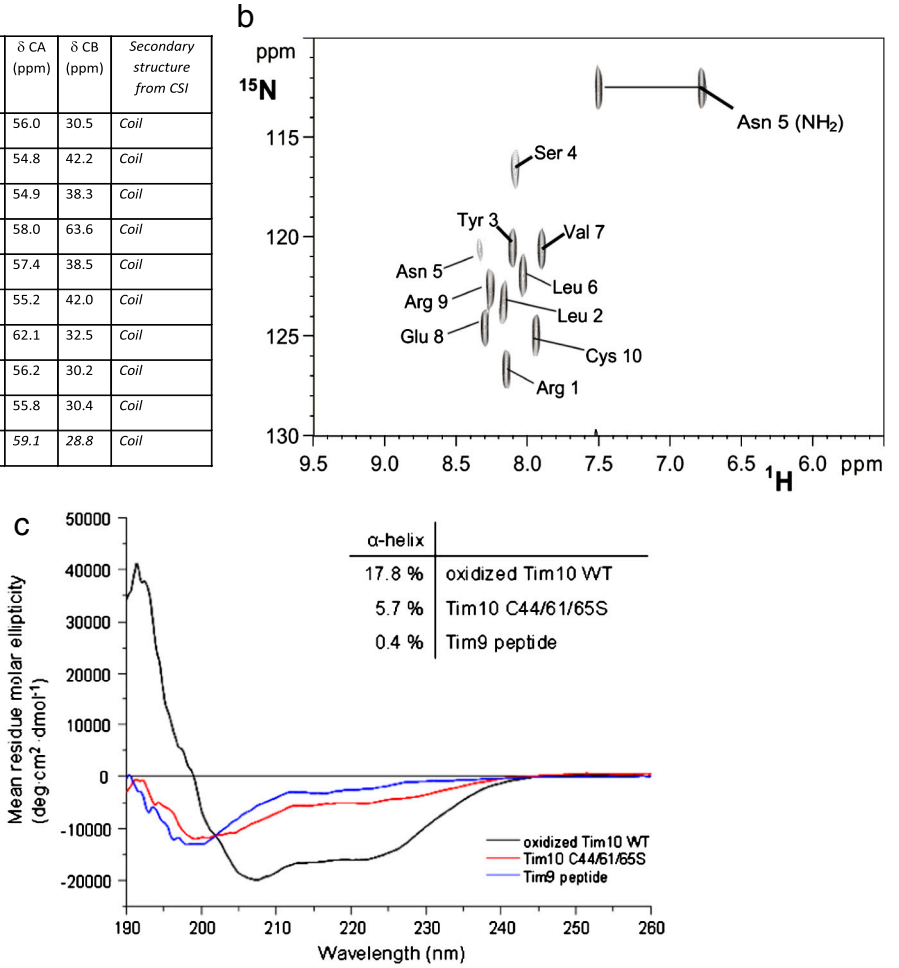

Fig. S4. Structural analysis of yTim9 peptide. (*A*) Secondary structure elements of yTim9 peptide as obtained from chemical shift index analysis; (*B*) ^{1}H-^{15}N HSQC map of yTim9 peptide. NHs chemical shift assignment is reported; (*C*) CD spectra of wild-type yTim10 (10 μM, black line), C44/61/65S yTim10 (10 μM, red line), and yTim9 peptide (100 μM, blue line). The samples were in 50 mM phosphate buffer, EDTA 0.5 mM, pH 7.0. The *Inset* shows the α-helical content of the three species, calculated from the ellipticity at 222 nm with the DICROPROT software package.

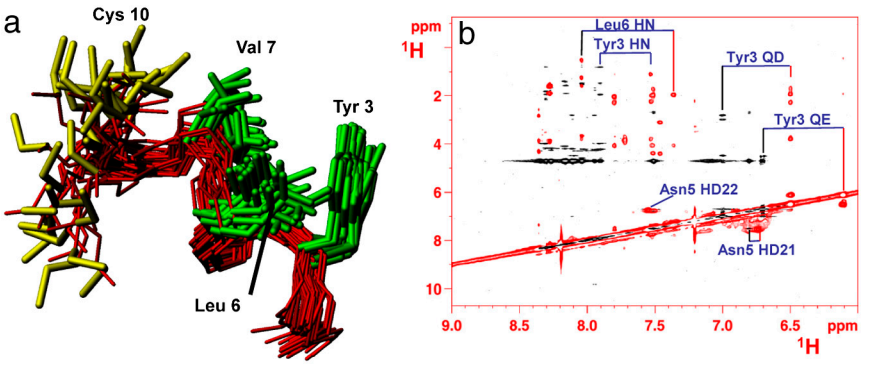

Fig. S5. Structural conformation of yTim9 peptide covalently complexed with C53S hMia40. (*A*) Bundle of the best 20 CYANA conformers (backbone in red) is shown. Side chains of the cysteine residue involved in the intermolecular disulfide formation with C53S hMia40 (yellow) and of the hydrophobic residues constituting the ITS of yTim9 (green) are shown. (*B*) 2D [^{1}H,^{1}H]-NOESY spectra of free yTim9 peptide (black) and of yTim9 peptide covalently complexed with C53S hMia40 (red). ^{1}H chemical shift variations of protons of Tyr3, Leu6, and Asn5, the first two residues belonging to the ITS of yTim9, are indicated.

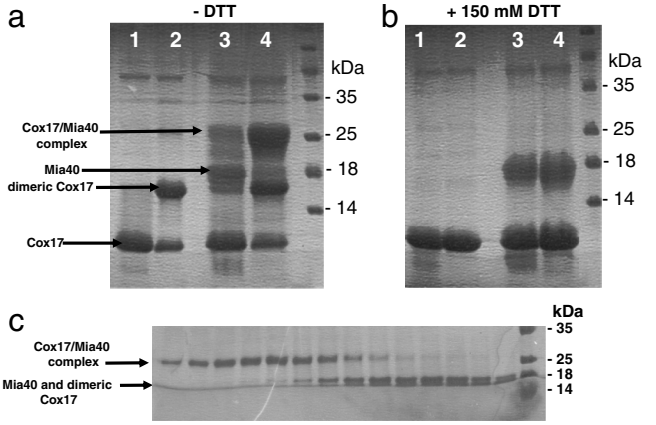

Fig. S6. Detection and purification of the covalent complex between C53S hMia40 and C26/36/55S hCox17. (*A*) Nonreducing SDS-PAGE of C26/36/55S hCox17 exposed to O_2 (1), C26/36/55S hCox17 with 5 mM ferricyanide $[Fe(CN)_6]^{3-}$ (2), a 2:1 mixture of C26/36/55S hCox17 and C53S hMia40 exposed O_2 (3), and a 2:1 mixture of C26/36/55S hCox17 and C53S hMia40 with 5 mM ferricyanide $[Fe(CN)_6]^{3-}$. (*B*) DTT-reducing SDS-PAGE of *A*. (*C*) Fractions of the C53S hMia40-C26/36/55S hCox17 covalent complex from the gel filtration column analyzed by nonreducing SDS-PAGE.

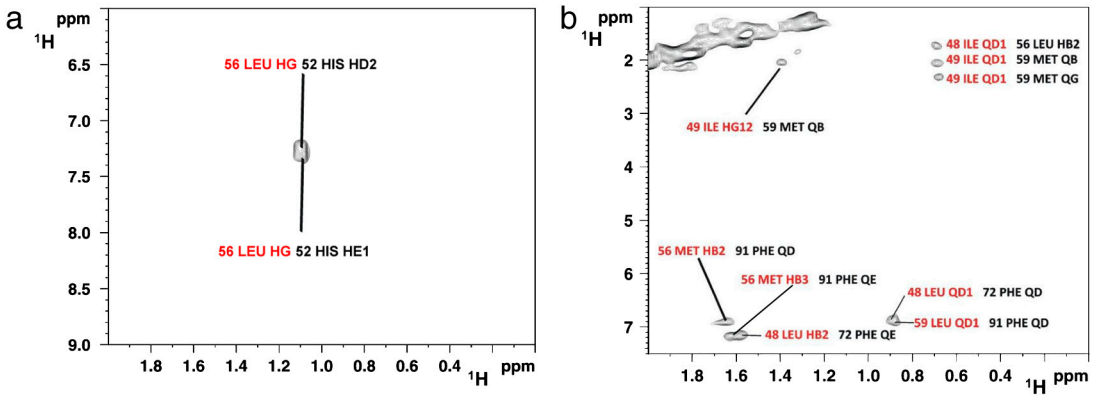

Fig. S7. Details of ω1-^{13}C-edited, ω2-^{13}C-filtered NOESY experiments in a 2D plane (^{1}H-^{1}H plane) of C26/36/55S hCox17-C53S hMia40 complex acquired on two samples. (*A*) ^{13}C,^{15}N C26/36/55S hCox17/unlabeled C53S hMia40 and (*B*) ^{13}C,^{15}N C53S hMia40/unlabeled C26/36/55S hCox17. The assignment of NOE cross-peaks is shown, indicating the resonances of the labeled and unlabeled proteins in black and red, respectively.

Table S1. NMR constraints and structural statistics of the hMia40/hCox17 complex

Distance and angle dihedral angle constraints	
Distance constraints	
Total NOE	1,375
Intraresidue	230
Interresidue	1,145
Sequential ($\|i-j\|=1$)	426
Medium-range ($\|i-j\|<4$)	452
Long-range ($\|i-j\|>5$)	255
Intermolecular	12
Hydrogen bonds	30
Angle constraints	
Total dihedral angle restraints	94
φ	47
ψ	47
Structure statistics	
Violations (mean ± SD)	
Distance constraints, Å	0.014 ± 0.001
Max. distance constraint violation, Å	0.022 ± 0.001
Dihedral angle constraints, °	2.834 ± 1.670
Max. dihedral angle violation, °	6.339 ± 2.537
Deviations from idealized geometry	
Bond lengths, Å	0.014 ± 0.001
Bond angles, °	2.200 ± 0.057
Impropers, °	9.583 ± 0.920
Average pairwise rmsd,* Å	
Backbone	0.81 ± 0.19
Heavy	1.13 ± 0.15
Ramachandran analysis	
Residues in the favored region, %	81.1
Residues in the additional allowed regions, %	15.3
Residues in generously allowed regions, %	2.7
Residues in disallowed regions, %	0.9

*Pairwise rmsd was calculated among 30 refined structures.

Table S2. Structural statistics of the experimental data-driven docking between hMia40 and yTim9 peptide

	C53S hMia40/yTim9 peptide complex *
Number of ambiguous interaction restraints (AIRs)	
Total AIRs	42
Number of AIR violations†	
Total AIR violations	6
Intermolecular energies after water refinement,† kcal mol^{-1}	
Haddock score	−79.3 ± 1.4
Van der Waals	−33.8 ± 2.2
Electrostatic	−205.7 ± 7.0
Desolvation	−8.5 ± 2.9
Restraints violations	41.4 ± 2.02
Buried surface area,† $Å^2$	1,247.6 ± 30.6
Deviations from idealized geometry†	
Bond lengths, Å	0.003 ± 0.000
Bond angles, °	0.45 ± 0.02
Impropers, °	0.41 ± 0.02
Dihedrals, °	25.3 ± 1.2
Average pairwise rmsd,† Å	
Backbone all	0.76 ± 0.40
Backbone interface	0.73 ± 0.37
Ramachandran analysis‡	
Residues in the favored region, %	84.0
Residues in the additional allowed regions, %	15.6
Residues in generously allowed regions, %	0.2
Residues in disallowed regions, %	0.2

*Docking models were ranked based on the average HADDOCK score. All 200 calculated structures were clustered in a single ensemble.

†Energetic and structural parameters calculated among the 200 refined structures.

‡Ramachandran analysis calculated among 30 refined structures.